Lattice theory of ultrafast excitonic and charge-transfer dynamics in DNA

ARTICLE *in* THE JOURNAL OF CHEMICAL PHYSICS · OCTOBER 2006

Impact Factor: 2.95 · DOI: 10.1063/1.2335452 · Source: PubMed

1 AUTHOR:

Eric R Bittner
University of Houston
128 PUBLICATIONS **2,035** CITATIONS

SEE PROFILE

Lattice theory of ultrafast excitonic and charge-transfer dynamics in DNA

Eric R. Bittner
Department of Chemistry and the Texas Center for Superconductivity, University of Houston, Houston, TX 77204
(Dated: June 8, 2006)

We propose a lattice fermion model suitable for studying the ultrafast photoexcitation dynamics of ordered chains of deoxyribonucleic acid (DNA) polymers. The model includes both parallel (intrachain) and perpendicular (cross-chain) terms as well as diagonal cross-chain terms coupling neighboring bases. The general form of our Hamiltonian is borrowed from lattice fermion models of quantum chromodynamics. The band-structure for this model can be determined analytically and we use this as a basis for computing the singly excited states of the poly(dA)poly(dT) DNA duplex using configuration interaction (CIS). Parameters for the model are taken from various literature sources and our own ab initio calculations. Results indicate that the excited states consist of a low energy band of dark charge-separated states followed by separate bands of delocalized excitonic states which have weak mixing between the thymidine and adenosine sides of the DNA chain. We then propose a lattice exciton model based upon the transition dipole-dipole couplings between bases and compare the analytical results for the survival probability of an initially localized exciton to exact numerical results. The results herein underscore the competing role of excitonic and charge-transfer dynamics in these systems.

I. INTRODUCTION

DNA is a remarkable molecule. With its four base-pairs, adenosine (A), thymidine (T), guanosine (G), and cytidine (C), the code of life is spelled out in all living organism on our planet. In each and every cell in the human body, there is approximately 1.7 meter of DNA strands that give the detailed instructions for how a cell is to operate, regenerate, build new cells, and eventually die. DNA also has a remarkably large photo-absorption cross-section for UVB (290-320 nm) radiation, making it susceptible to carcinogenic mutations. By an large, the primary photochemical product of UV radiation in this region is the formation of cyclobutane pyrimidine dimers and pyrimidine (6-4) pyrimidone photoproducts. In the case of the cyclobutane pyrimidine dimers, neighboring thymidine bases become co-joined lesions within the DNA strand. The distribution of lesions depends strongly upon the sequence, suggesting some degree of electronic coupling between bases.[1] Such cooperative coupling could initiate a series of events through the formation of Franck-Condon states delocalized over several bases[2]. Yet, the DNA ultraviolet absorption spectra seems to closely resemble sum of the spectra of the individual base pairs–suggesting the initial excitons are localized on individual bases. Work by Kohler's group indicates that base-stacking, rather than interbase coupling plays the dominant role in the excited state dynamics of poly(dA)-poly(dT) duplex chains.[3] More recent theoretical calculations on model double helices indicate that the excited states are delocalized over a bases and that there is only a slight spectral shift with respect to the non-interacting monomers and in agreement with experimental spectra.[4, 5] Finally, fluorescence upconversion and time-correlated single photon counting probes of double helix poly(dA)-poly(dT) indicate that the spectral properties of the duplex can not be explained by photon absorption of a single adenine or thymine base, but can only be explained by the formation of delocalized excited states followed by energy transfer via intraband scattering on a timescale of less than 100 fs.[2] However, ab inito MD simulations of poly(dA)-poly(dT) indicate that the relevant electronic states are localized due to structural changes promoted by thermal fluctuations. [6, 7, 8, 9]

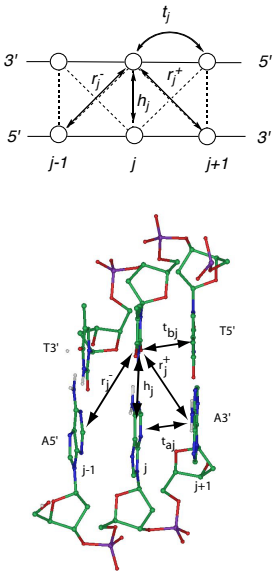

FIG. 1: (Top) Lattice fermion model for two chain dimer showing the connectivity implied by the various hopping terms. (Bottom) Mapping of lattice model onto $(dA)_3(dT)_3$ segment.

In this paper we develop a lattice model for exploring the excited state dynamics in double helix DNA chains.[1, 7, 10, 11, 12, 13, 14, 15, 16, 17, 18, 19, 20] Our work in this area draws upon our recent work in

developing similar models for the excitonic and charge-transfer dynamics in organic polymer semiconducting species. [21, 22, 23, 24, 25, 26] Indeed, we find many of the concepts from the field to be transferable to the study of the excited states DNA. Our model is based upon a localized description of the highest occupied and lowest unoccupied π and π^* orbitals on each base coupled via Coulomb and exchange interactions. The single particle operators include intra- and inter-chain electron and hole hopping between neighboring bases as well as interchain terms coupling next neighbor bases. The resulting single particle operator is identical to the Wilson lattice fermion model of quantum chromodynamics and we can analytically determine the pairs of conduction and valence bands along the chain. We also include dipole-dipole terms coupling excitonic configurations. The resulting eigenstates include both excitonic states localized to one chain or the other as well as lower lying charge-separated states and states which contain significant amount of interchain coupling. Finally, we consider the time-evolution of a localized excitonic state and it survival probability. To conclude, we comment upon recent ultrafast investigations of model DNA duplex chains and how the present model should be improved to include thermal fluctuations and vibrational relaxation processes.

II. THEORETICAL TREATMENT

A. Lattice Fermion Model

In developing a localized model for molecules such as DNA, one needs to consider the hopping of an electron or hole between neighboring bases within the same strand, the hopping between base-pairs, as well as inter-strand coupling between consecutive bases.

To begin, let us define the following fermion operators, $a_j, a_j^\dagger$ and $b_j, b_j^\dagger$ which remove and create Fermions on the j^{th} lattice site on the "a" chain or on the "b" chain which respectively represent one chain or the other in the DNA double helix. These operators have the typical anti-commutation relations

$$\{a_j, a_k^\dagger\} = \delta_{jk} \;\; \& \;\; \{a_j, b_k\} = 0. \tag{1}$$

Using these operators we can write spinor operators as

$$\hat{\psi}_j \;=\; \begin{pmatrix} a_j \\ b_j \end{pmatrix} \tag{2}$$

$$\bar{\psi_j} \;=\; \hat{\psi}_j^\dagger \gamma_o \tag{3}$$

where γ_o is the 2×2 spin matrix

$$\gamma_o = \begin{pmatrix} 0 & 1 \\ 1 & 0 \end{pmatrix}. \tag{4}$$

The wave function on the lattice is then given by

$$|\psi\rangle = \sum_j \phi_j \hat{\psi}_j^\dagger |0\rangle \tag{5}$$

where ϕ_j is the spinor amplitude on the j^{th} site. If we neglect interchain transfers, then the single particle terms for the intra-chain hopping reads

$$h_1 = \sum_j \epsilon_j \hat{\psi}_j^\dagger \hat{\psi}_j + \sum_j t_j (\hat{\psi}_{j+1}^\dagger \hat{\psi}_j + \hat{\psi}_j^\dagger \hat{\psi}_{j+1}) \tag{6}$$

where ϵ_j and t_j are 2×2 diagonal matrices containing the site energies and transfer integrals at a given site index. The general topology of the lattice model is shown in Fig. 1. One can imagine that the connectivity corresponds to laying the helix out as a ladder with the base-pairs forming the rungs.

For a lattice modeling the DNA double helix, we consider essentially two types of interchain interactions. The first simply takes a particle at site j on one chain and transfers it to site j on the other chain. This term is given by

$$h_\perp = \sum_j h_j \bar{\psi}_j \hat{\psi}_j. \tag{7}$$

and describes the transfer of a quasi-particle (electron, hole, or excitation) from one base pair to the other. $h_\perp$ mixes the two spinor components and introduces a band-gap in the spectrum.

The second interchain hopping term can by included by having the interchain hop be associated with a "diagonal" transfer from site j to $j \pm 1$ as in

$$h_{diag} = \sum_j r_j (a_j^\dagger b_j + 1 + b_j^\dagger a_{j+1} + b_{j+1}^\dagger a_j + a_{j+1}^\dagger b_j) \tag{8}$$

which can be equivalently written as

$$h_{diag} = \sum_j r_j (\bar{\psi}_{j+1} \hat{\psi}_j + \bar{\psi}_j \hat{\psi}_{j+1}). \tag{9}$$

This is the so-called "Wilson" term for staggered fermions which removes most of lattice doubling of the quarks in quantum chromodynamics [27, 28] while retaining chiral symmetry. This corresponds to the transfer of a quasi-particle from a base on one chain to a base on the other chain displaced by ±1 site. This occurs in DNA because of the increased π overlap between interchain neighbors due to the helical twist of the chain itself. [29] Furthermore, this interaction depends upon whether the particle is moving in the 3' to 3' direction or in the 5' to 5' direction. With this in mind, we separate the h_{diag} into two components, one r_i^+ which transfers from site i on chain a to site $i+1$ on chain b (3' to 3' transfer) and the other (r_i^-) which transfers from site $i-1$ on chain b to site i on chain a (5' to 5' transfer),

$$h_{diag} = \sum_j (\hat{\psi}_{j+1}^\dagger (r_j^+ \gamma_+ + r_j^- \gamma_-) \hat{\psi}_j + h.c.). \tag{10}$$

When $r_j = r'_j$, $\gamma_+ + \gamma_- = \gamma_o$, we recover the original diagonal mixing term. As seen below, the mixing becomes momentum dependent.

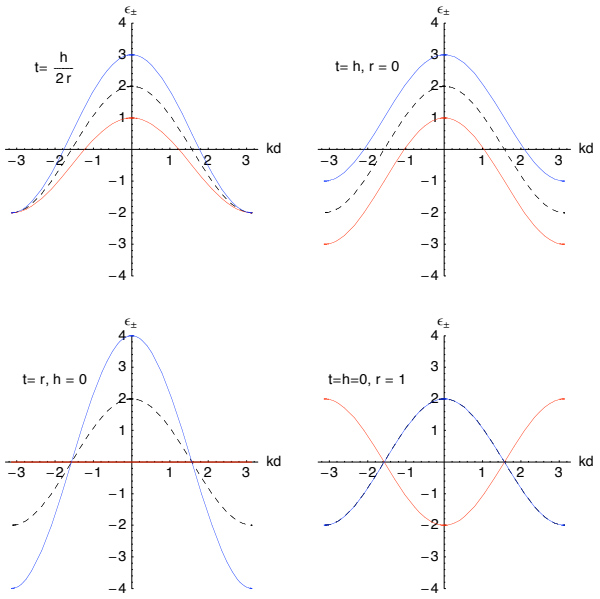

FIG. 2: Single particle energy bands of lattice model. The red and blue bands correspond to the separated bands while the dashed curve corresponds to the degenerate parallel lattice with $r = h = 0$.

TABLE I: Site energies and intrachain single particle matrix elements

	DGU	DCY	DAD	THY
ϵ_e	1.137	-1.065	0.259	-0.931
ϵ_h	-4.278	-6.519	-5.45	-6.298
t_e	0.019	-0.061	0.024	-0.023
t_h	-0.115	-0.024	0.021	-0.098

If we take the ideal case where ϵ_i, r_i, t_i, and h_i are constants and assume the lattice to be infinite, then we can write the single particle band operator h_i in the momentum representation as

$$\hat{h}(k) = \begin{pmatrix} \epsilon + 2t\cos(kd) & h + 2r\cos(kd) \\ h + 2r\cos(kd) & \epsilon + 2t\cos(kd) \end{pmatrix} \tag{11}$$

where $0 \leq kd \leq 2\pi$. From this, we can immediately determine the energy dispersion as

$$E_{\pm}(k) = \epsilon + 2t\cos(kd) \pm (h + 2r\cos(kd)) \tag{12}$$

The $E \pm (k)$ bands correspond to the two possible branches for the energy spectrum arising from the coupling of the two chains.

When h and r both vanish, and all the intrachain hopping terms are identical we recover the energy dispersion relation for the infinite lattice,

$$E(k) = 2t\cos(kd) + \epsilon \tag{13}$$

TABLE II: Interchain single particle matrix elements for poly(dG)poly(dC) and poly(dA)poly(dT) chains.

poly(dGdC)	e	h
h_i	0.063	0.002
r_i^+	-0.012	-0.007
r_i^-	-0.016	0.050
poly(dAdT)	e	h
h	0.034	0.026
r_i^+	-0.010	-0.011
r_i^-	-0.013	0.009

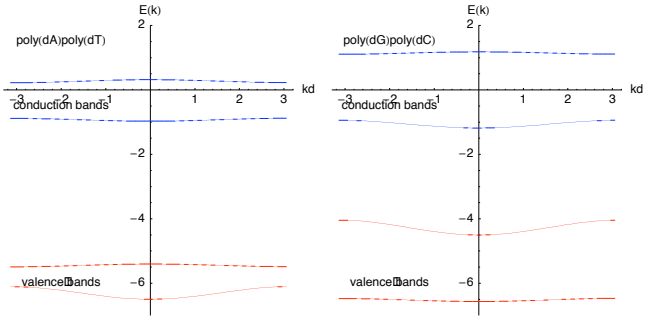

FIG. 3: Valence and conduction bands of extended poly(dA)poly(dT) and poly(dG)poly(dC).

where $0 \leq kd \leq 2\pi$ and d the lattice spacing. In this limit the electron or hole wavefunctions are delocalized Bloch states with well-defined momentum k. Both the h and r terms lift the degeneracy of the branches at various points along the Brillouin zone and we show a select set of cases in Fig. 2. If we include the hopping across base pairs, the energy dispersion reads

$$E(k) = 2t\cos(kd) + \epsilon \pm h \tag{14}$$

and we have two parallel bands separated by $2h$ at every value of k. Of particular note is when

$$\frac{h}{2r} = 1 \tag{15}$$

in which the gap between the two bands close at $k = \pm\pi$. In lattice fermion models of quantum chromodynamics, this corresponds to the case in which one obtains massless pions. A second interesting case is where $t = r$ but $h = 0$ in which one obtains increased mobility in one band, but completely localized species in the other.

Finally, if we include the distinction between 3'-3' hopping and 5'-5' hopping, the single particle band operator becomes

$$\hat{h}(k) = \begin{pmatrix} \epsilon_a + 2t_a\cos(kd) & h + r_+e^{-ikd} + r_-e^{+ikd} \\ h + r_+e^{+ikd} + r_-e^{-ikd} & \epsilon_b + 2t_b\cos(kd) \end{pmatrix}. \quad (16)$$

where $\epsilon_{a,b}$ and $t_{a,b}$ are the site energies and parallel hopping terms for the two bands.

In Fig. 3 we show the resulting four conduction and valance bands for both poly(dA)poly(dT) and poly(dG)poly(dC) using the parameters given in Tables I and II. For the poly(dA)poly(dT) case, to lowest order approximation one can assign the four separate bands as being the valence bands of the thymindine and adenosine chain respectively for the lowest two bands and as the condiction bands of the thymidine and adenisine chain respecitively for the upper two bands. Likewise for poly(dG)poly(dC). The two lowest energy bands correspond to the valence bands of cytosine and guanosine respectively while the two upper bands correspond to the conduction bands of cytosine and guanosine. In solid-state physics, such an arrangement of bands is termed a type-II heterojunction and the electronic properties of such systems are very sensitive to the off-set between the bands from each domain and the strength of the electron/hole Coulombic interaction.

It is interesting to note that in both cases, valance band holes are considerably more mobile than conduction electrons. Furthermore, with the exception of the valence bands of poly(dA)poly(dT), the bands are relatively well separated in energy consistent with fact that hole and electron transport in DNA is dominated by intra-strand transport.

In order to generate a minimal model for the excited states of a DNA chain, we need to make a number of judicious assumptions. The first and foremost is that the highest occupied and lowest unoccupied π and π^* molecular orbitals of each isolated base define the localized orbitals of the bases in the DNA chain itself. One can then directly compute the Coulomb and exchange interactions between orbitals localized on different bases. For poly(dA)-poly(dT) and poly(dG)-poly(dC) in the B form of the double helix, these interactions have been reported by Mehrez and Anantram [30] for the electron and hole hopping integrals and are reproduced here in Tables I and II. The corresponding conduction and valance bands for the infinitely extended poly(dA)-poly(dT) and poly(dG)-poly(dC) chains are shown in Fig. 3. In general the two conduction and two valence bands are well separated in energy. The localization or delocalization of these states is determined by the widths of these bands. In poly(dG)-poly(dC), the upper valence band corresponds to delocalized hole states along the guanosine side of the chain. Since, $t_h = -0.115$ eV, the delocalized states at $k = 0$ are lower in energy. The remaining bands are far narrower and hence support localized electron or hole states. This is consistent with fact that conduction in poly(dG)-poly(dC) is largely dominated by hole transport along the π stacked guanosine units. In poly(dA)-poly(dT), hole motion along the thymidine would be quite facile except for the fact that energically the hole prefers to be on the adenisine chain. The remaining bands are very narrow and transport in these band should be dominated by incoherent hopping between localized sites rather than by coherent means (i.e via delocalized orbitals).

For an interacting model, we need to include spin-dependent two particle coupling terms of the form

$$V^T_{mn} = -\langle m\overline{n}||n\overline{m}\rangle \quad (17)$$

$$V^S_{mn} = V^T_{mn} + 2\langle m\overline{n}||\overline{m}n\rangle. \quad (18)$$

for triplet and singlet combinations respectively with

$$\langle m\overline{n}||i\overline{j}\rangle = \int d1 \int d2\phi^*_m(1)\phi^*_{\overline{n}}(2)v(12)\phi_i(1)\phi_{\overline{j}}(2) \quad (19)$$

where the state $|m\overline{n}\rangle$ refers to an electron/hole configuration with an electron localized on the mth base and a hole localized on the nth base. With the exception of geminate bases, orbital overlap is small such that the two-body interactions are limited to Coulomb, $J(r)$, and exchange integrals, $K(r)$, reflecting e-h attraction and spin-exchange coupling non-geminate configurations. For convenience, we take the Mataga form of these integrals as used in our previous works with

$$J(r) = J_o/(1 + r/r_o)$$

and

$$K(r) = K_o e^{-r/r_o}$$

taking r to be the linear distance between the centers of the 6-membered rings on each base. These are very local interactions coupling primarily π-stacked base pairs. [26] For these interactions, we adopt simple parametric forms as used in our previous works in which the direct and exchange interactions is taken to be very short ranged and limited to at most nearest neighbors (see Table III). We take the on-site Coulomb interaction to be 2.5eV and on-site exchange interaction to be 1.0eV.

In addition, for singlet states we include dipole-dipole coupling terms that correspond to the interchange of geminate electron-hole pairs between separated sites. Typically, excitation energy is transferred at distances R far shorter than the wavelength of light λ corresponding to the given transition. For distances $R > a$ where

a is the size of the molecule, we can employ a multipole expansion in which the lowest order term corresponds to the coupling between dipoles. Multipole and exchange terms become important at small distances or when the dipole transitions are forbidden by symmetry.

The interaction energy between two dipoles is given by

$$M = \frac{1}{R^3}(\vec{\mu}_a.\vec{\mu}_b - \frac{3}{R^2}(\vec{\mu}_a\vec{R})(\vec{\mu}_b\vec{R}))$$

where $\vec{\mu}_{a,b}$ are the transition dipole moments of A and B and $\vec{R}$ is a vector separating the two. This is also referred to as the point-dipole approximation and we use this to provide an estimate of the dipole-dipole coupling between excitonic configurations. This is probably the most severe of the approximations we have made thus far since the intrachain stacking distance of 3.4 Å is clearly on the order of the molecular dimension and hence higher order terms in the multiple expansion should be included.[10]

To determine these terms, we computed the transition dipole moments between the vacuum state $|0\rangle$ and the localized $\pi - \pi^*$ state by performing single configuration interaction calculations for the isolated bases using the GAMESS [31] quantum chemistry package. For this, we modeled the deoxynucleosides using the corresponding 9-methylated purines or 1-methylated pyrimidines optimizing the geometries using Hartree Fock and the 6-31(d)G basis. We then converged the lowest 10 singlet excited states using configuration interaction (CIS). The transition moments and oscillator strengths are tabulated in Table IV. These compare well with previous reported values from both theory and experiments in Refs.[10, 32] The interested reader is referred to these papers for an excellent discussion of the excited states of the DNA bases. It should be noted that the *ab initio* excitation energies reported in Ref. [32] are rescaled by a factor of 0.72 to account for the difference in electron correlation between the ground and excited states. Here, we report the actual calculated values. We also note that this issue of how electron correlation is treated will also affect the magnitues of the transition dipole moments.

We then translated and rotated these moments onto the individual bases in the DNA chain to generate the transition dipole operator for the DNA molecule itself. This effectively incorporates the specific structural and configurational details into the transition dipole operator as illustrated in Fig. 4. In each case, the transition moments with the largest oscillator strengths are more or less parallel to the C4-N1 axes in guanosine and adenosine and to the C6-N3 axes in thymidine and cytidine, which implies that within the DNA chain itself, these moments point towards the axial center of the double helix. These are illustrated in Fig. 4 in which we take poly(dA)$_{10}$poly(dT)$_{10}$ in its B-DNA form and superimpose the transition dipoles. For points of reference, the loci in this figure correspond to the mid-point between the C4-N1 and C6-N3 atoms.

In Fig. 5 we show the full dipole-dipole coupling matrix for the (dA)(dT) duplex, listing the nearest-neighbor intra-chain, inter-base perpendicular, and inter-base diagonal terms in in Table V. All diagonal terms are all zero. Furthermore, the coupling is strongest between adjacent base pairs followed by coupling between nearest neighbors on the same chain and nearest neighbors in the other chain dying off rapidly beyond that. The matrix elements themselves span a range between 0.143 eV for the $d_{\|}^T$ terms to -0.013286 for the d^+ diagonal cross-chain mixing terms. Systematically, these values are greater in magnitude than those reported by Bouvier *et al.* [10] The overestimation of the coupling is certainly due to our use of the point-dipole approximation and our use of the CIS approximation.

The sign and magnitude of each term largely reflects the geometric arrangement of the bases along the DNA chain. The perpendicular coupling term $d_\perp < 0$ owing to anti-parallel arrangement of the transition dipoles on the base pairs. This term is nearly an order of magnitude less than the d^+ term which couples bases diagonally across the lattice in the 3'-3' direction. The dominant

TABLE III: Electron/hole interactions.

Term	Functional form	Parameters
Direct Coloumb	$J(r) = J_o/(1 + r/r_o)$	$J_o = 2.5$ eV
		$r_o = 1.0$Å
Exchange	$K(r) = K_o e^{-r/r_o}$	$K_o = 1.0eV$
		$r_o = 0.5$ Å

Note: a = unit lattice spacing.

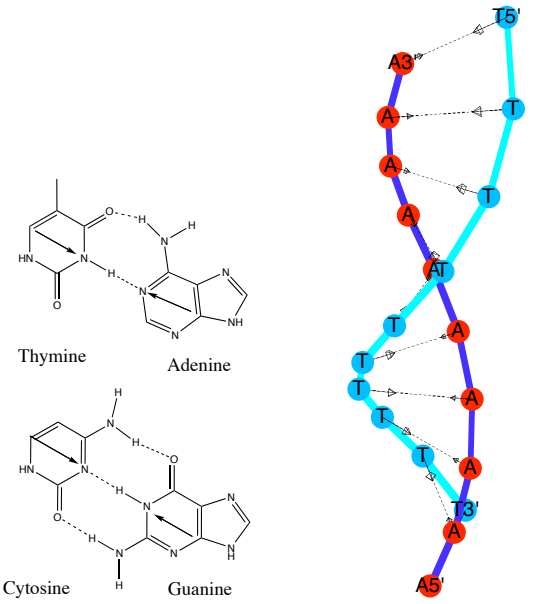

FIG. 4: (Left)Watson-Crick base pairs of DNA. (Right) Geometry of poly A$_{10}$-poly T$_{10}$ sequence. Arrows indicate direction of the $\pi - \pi^*$ transition dipoles for each base.

TABLE IV: Transition dipole components (in e-Å), energies, and oscillator strengths for lowest singlet excited states of each isolated base computed using HF/6-31G/CIS. Note that values in parenthesis should be read as $(x) = 10^x$. Note also that in contrast to previously reported transition energies, we do not rescale our energies.

Base	μ_x	μ_y	μ_z	$\lvert\mu_{0n}\rvert$	E(eV)	f_{0n}
A(0-1)	-1.02	-0.194	9.95(-3)	1.04	6.60	0.174
A(0-2)	1.15	-0.235	-6.84(-3)	1.174	6.63	0.224
A(0-3)	8.24(-3)	-0.0134	0.0570	0 .0592	7.21	6.18(-4)
T(0-1)	-8.34(-3)	4.04(-3)	-0.0344	0.0356	6.46	2.00(-4)
T(0-2)	-1.67	0.570	-2.20(-3)	1.77	6.62	0.505
T(0-3)	5.74(-3)	-0.0275	0.0131	0.03102	7.88	1.86(-4)
G(0-1)	0.559	1.10	-2.62(-3)	1.23	6.14	0.229
G(0-2)	-5.30(-3)	-1.04(-4)	-0.0675	0.0678	6.78	7.63(-4)
G(0-3)	1.36	-0.0431	3.652(-3)	1.36	7.21	0.325
C(0-1)	0.934	0.587	6.72(-3)	1.10	6.22	0.185
C(0-2)	-0.0529	0.0360	0.132	0.147	6.92	0.004
C(0-3)	-0.0378	-0.0371	0.0484	0.0718	7.34	0.001

TABLE V: Local Dipole-Dipole couplings for (dA)(dT). Note that the last two values correspond to the energy required to place a localized exciton on a single site along either the dT or dA chain as computed using the full CI Hamiltonian of a 10-base-pair (dA)(dT) chain.

$$d_\perp = \text{-0.009858 eV}$$
$$d^- = \text{-0.006342 eV} \quad d^+ = \text{-0.013278 eV}$$
$$d_\parallel^A = 0.069758 \text{ eV} \quad d_\parallel^T = 0.143087 \text{ eV}$$
$$\epsilon_A = 5.209 \text{ eV} \qquad \epsilon_T = 4.867 \text{ eV}$$

terms, however, are the parallel coupling terms, $d_\parallel^{A,T}$, that couple base-stacked units on the same side of the chain.

As in the single particle case, one can define quasi-particles in terms of excitons and arrive at a similar lattice fermion model with a quasi-particle hamiltonian given by Eq. 16 with $t_{A,T} = d_\parallel^{A,T}$, $h = d_\perp$, $r^+ = d^+$, and $r^- = d^-$ (See Table V for numerical values). The resulting exciton band structure for the extended (dA)(dT) duplex is shown in Fig. 8. All in all, the band structure is predominantly that of two isolated bands of free excitons localized on either the T (lower band) or A (upper band) side of the DNA strand.

The structure of the purely excitonic band-structure is very much in contrast with our previous discussion of the CI eigenstates. For the adenosine band (the upper curve), the state at $k = 0$ is the delocalized exciton. As $|k|$ increases, the wavelength of the state decreases, and more nodes appear in the wavefunction. This is consistent with the eigenstates we compute using the CIS Hamiltonian. On the other hand, for the thymidine band (the lower curve), the CIS eigenstates have the longest

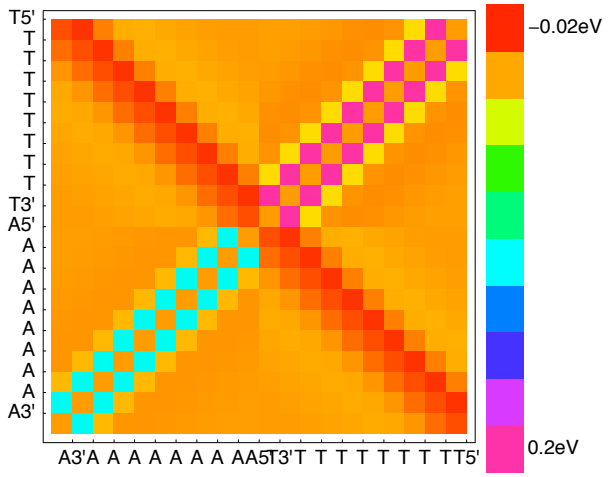

FIG. 5: Dipole-dipole coupling matrix for the (dA)(dT) duplex. As indicated by the scale to the right, a matrix element with a value of zero is indicated by an orange coloration.

wavelength thymidine exciton as the lowest energy exciton with progressively short wavelength translational excitations lying higher in energy. Based upon the CIS states, one would expect then that the lower exciton band would be the mirror image of that seen in Fig. 8. i.e. with the band minimum at $k = 0$ and maxima at $k = \pm\pi/d$.

B. Excitonic and Charge Transfer States of $(dA)_{10}(dT)_{10}$ DNA Duplex

To test the parameterization of the model, we compute the absorption spectrum of poly$(dA)_{10}$poly$(dT)_{10}$ in the B helical form. For this we computed the singlet CI states of the poly$(dA)_{10}$poly$(dT)_{10}$ chain and used the transition dipoles from the quantum chemistry calculations to estimate the oscillator strength of each state. The states were then convoluted with a Lorenzian line-shape function with a 20 nm width. The predicted spectrum shown in Fig. 7 has one main peak centered at at 265nm composed of transitions from the lowest three excitonic states along the thymidine side of the DNA chain at 4.68 eV, 4.77eV, and 4.93 eV respectively (276.4nm, 271.2 nm and 262.3 nm). These correspond to translational excitations of the exciton center of mass along the thymidine chain. The full density of excited states is shown in the right-hand figure of Fig. 7. States in the gray-shaded region are charge separated states with the holes on the thymidine side and the electrons along the adenosine side of the chain.

The position of the absorption peak is quite sensitive to magnitude of the on-site Coulombic interaction. We systematically adjusted this term (J_o) as to center this peak to reproduce the aqueous phase UV spectrum of thymine and adenine. [33] This is also consistent with results re-

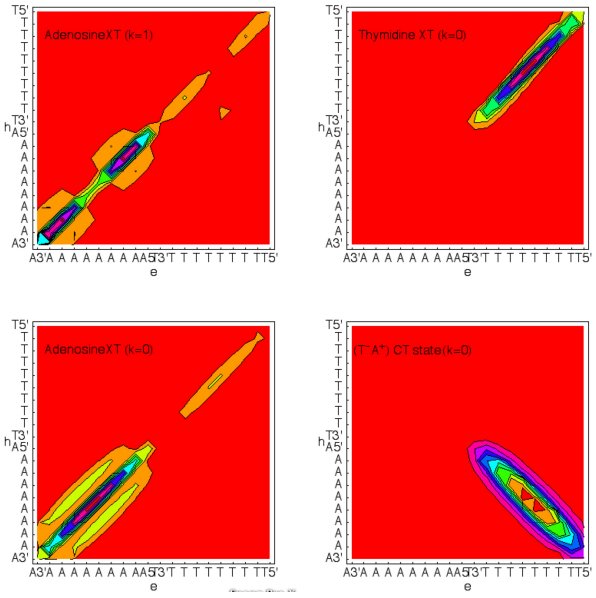

FIG. 6: Sampling of some of the relevant CI states for the $(dA)_{10}(dT)_{10}$ chain. Please refer to the text for details and discussion.

ported by Emanuele, et al. for the UV spectra of the $(\mathrm{dA})_{10}(\mathrm{dT})_{10}$ duplex[4, 5] For fluorescence studies of the nucleic acid bases and related heterocyclic compounds, see Ref. [34]. While we do not address the transient fluorescence in this paper, we shall in subsequent works.

A representative sampling of the CIS eigenstates are given in Fig. 6. The first state we note is the thymidine exciton (with $k = 0$) which has energy 4.58 eV. This is a delocalized long-wavelength excitonic state as evidenced by the fact that it is primarily composed of geminate electron hole pairs. This state has the largest transition moment to the ground-state and is the lowest lying state with any appreciable coupling to the ground state.

The fully delocalized adenosine exciton occurs at 5.36 eV (241.336 nm). Much like the thymidine exciton, this is essentially the translational eigenstate of the electron/hole pair confined to a one-dimensional box. Remarkably, the two states *lower* in energy are also translational eigenstates, however, with 1 and 2 nodes along the adenosine chain. In Fig. 6 we show one of these (denoted $k = 1$) which has a single node along the adenosine chain and and energy of 5.35 eV. The reflects the fact that both the single particle and adenosine exciton quasi-paricle bands (as discussed below) all have negative curvature at $k = 0$. Hence, any translational excitation with $|k| > 0$ must be correspondingly lower in energy. The excitons along the thymidine side are more typical since the valence and bands conduction have positive curvature at $k = 0$ and hence translational excitations are higher in energy.

We next turn our attention towards the charge separated states. There are essentially two types of charge-separated states. One, in which the electron and hole are not on the same base, but remain along the same chain (intrachain charge separation) and a second in which the electron and hole are on different chains (interchain charge separation). The interchain charge separated states lie energetically below the thymidine exciton at 4.58 eV. The lowest few states correspond to the electron and hole moving in parallel along the DNA chain, with the electron along the adenosine and the hole along the thymidine chains. The interchain charge-separated states are lower in energy than the intrachain charge-separate states. The lowest of which is shown in Fig. 6. Between this state and the lowest thymidine exciton are 100 charge-separated states of various complexity.

The intrachain charge-separated states correspond to antisymmetric linear combinations of electron-hole configurations along a given chain resulting in a node along the electron/hole separation coordinate, such as

$$|CT\rangle = \sum_i c_i(|e_{i-1}h_{i+1}\rangle - |e_{i+1}h_{i-1}\rangle).$$

From such states, we define the intrachain exciton binding energy as the energy difference between the lowest antisymmetric and lowest symmetric state with regards to exchange of the electron and hole. For the case at hand, we get $\epsilon_B = 0.13eV$ along the thymidine chain and $\epsilon_B = 0.15$eV along the adenosine chains. These are lower than the typical exciton binding energies of about 0.5eV found in conjugated polymer species.

This sampling of states is by no means complete since a comprehensive study of the spectroscopy and excited states of DNA must include some measure of the thermodynamic disorder and structural fluctuations of the molecule itself. So far as ultrafast dynamics is concerned, we have clear separation of time scales between the structural and thermal motions of the chain and the electronic transfer between bases. Hence, we assume that the electronic dynamics along the chain occur in fixed nuclear frame. The results here serve as a benchmark of our approach and provide a starting point for discussing the ultrafast dynamics of energy transfer and migration immediately following photo-excitation. We now turn our attention towards such dynamics.

III. EXCITONIC DYNAMICS

Recent ultrafast studies of DNA duplexes has begun to illuminate the competition between base-stacking and cross-chain interactions in the dynamics of photoexcited states. One one hand, disorder in the chain itself leads to localized excitonic states and hence should limit the extent of coherent transport along the chain due to *pi* stacking of the bases. Furthermore, the off-set between the HOMO or LUMO energy levels on adjacent bases is generally greater than the exciton binding energy. In the case at hand, these binding energies are estimated to be around 0.13 eV whereas the energy difference between adjacent HOMO levels in, say, adenosine and thymidine

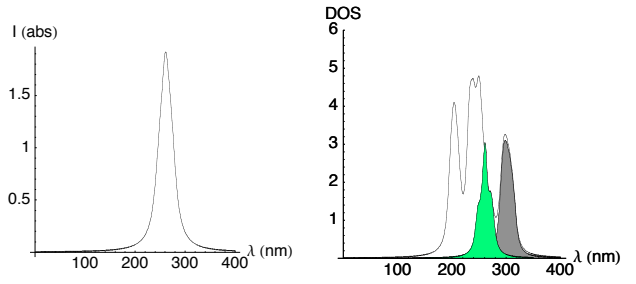

FIG. 7: (Left)Absorption spectrum of poly(dA)poly(dT) based upon lattice hopping model. (Right) Density of singly excited state for poly(dA)poly(dT). The dark shaded regions correspond above 300nm correspond to the low-lying charge-separated states. The green-hued region is the density of states scaled by the oscillator strength and indicating the optical excitonic bands.

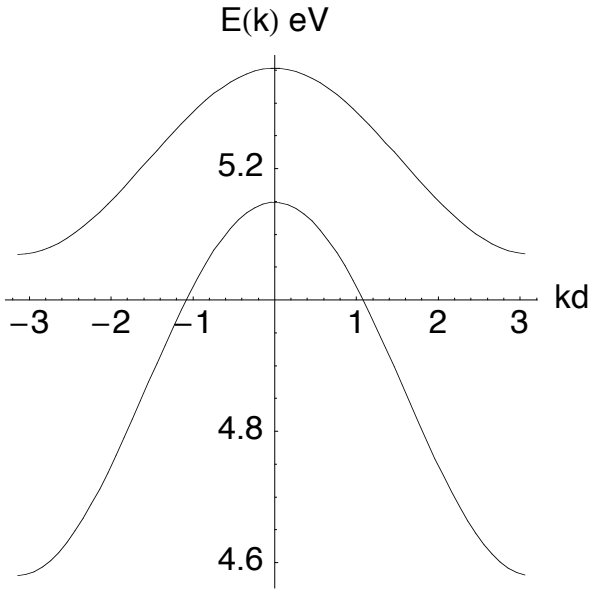

FIG. 8: Excitonic band structure for extended (dA)(dT) duplex based upon lattice fermion model and dipole-dipole coupling terms.

is 1.3 eV. Even if the exciton binding energy were much stronger, which would result in a dramatic shift to the red of the absorption spectrum due to the increased stability of the excitonic state, one has the classic type II heterojunction arrangement of energy bands commonly found in photovoltaic cells. In the case of DNA, the heterojunction is along the helical axis itself with the two parallel chains forming two quasi-one dimensional semiconducting domains. In such systems, fluorescence should be immediately quenched by exciton dissociation in to radical cation/anion pairs in which the charge carriers may be weakly bound at the heterojunction between the two semiconducting domains. In contrast, when the exciton binding is greater than the HOMO or LUMO offset at the heterojunction, excitons are the energetically favored species and fluorescence with very high quantum yields is likely to occur. Such is the case of certain organic light-emitting diodes fabricated using phase segregated polymer semiconducting materials with band-off sets close to the exciton binding energy.

Since we are dealing primarily with electronic excited states that are extended along the DNA duplex, we shall assume at the present time that the electronic dynamics occur in the fixed framework of the nuclear coordinates. That is to say that while conformational fluctuations with in the chain play a significant role in determine the matrix elements of our electronic Hamiltonian, the elements remain static over the initial time scale of the electronic evolution. Taking the B DNA helix to be statistically the average structure of the duplex DNA in aqueous solution, we can assume that the matrix elements given here are statistical mean couplings. Fluctuations within the structure should lead to fluctuations about these mean couplings and one can in fact develop random Hamiltonian models for studying the role of fluctuations in determining the quantum transport properties in such systems. [35]

A. Survival of a Localized Exciton in dAdT

We begin by considering the fate of a localized exciton placed on the single base. This is a nonstationary state and will evolve under the time-dependent Schrödinger equation

$$i\hbar\frac{\partial}{\partial t}\psi(t) = H|\psi(t) \tag{20}$$

where H is the CI hamiltonian described in the previous section. Since we already have the CI eigenstates, it is trivial matter to evolve any initial state in time using the Tchebychev propagation methods that preserve the total norm and total charge of the system.[36]

If we invoke the modified ladder model above, the survival probability of an exciton quasi-particle placed on the nth thymidine site is given by

$$S_n(t) = \left|\left(\frac{1}{2\pi}\int_{-\pi}^{\pi} e^{-ih(k)t/\hbar}dk\right)_{11}\right|^2 \tag{21}$$

where the integral is over the first Brillouin zone and $h(k)$ is the band operator of Eq. 16. In Fig. 9 we compare the survival probability of a localized thymidine exciton as given by the full exciton model which includes the charge-separated states and the analytical exciton band model that includes only the nearest neighbor dipole-dipole coupling terms. Remarkably, the band model gives a strikingly good description of the survival probability indicating that the first few recurrences are due to exciton transfer to and from the neighboring sites and are not due to the finite size of the system; although, after about

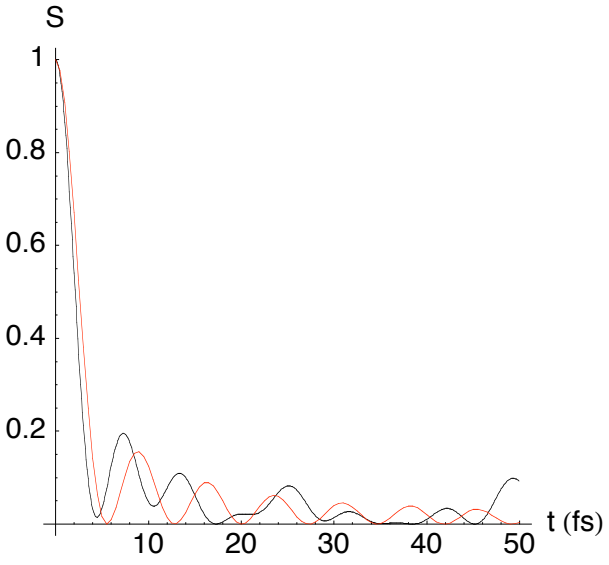

FIG. 9: Comparison between numerical survival probability (black) and analytical survival probability (red).

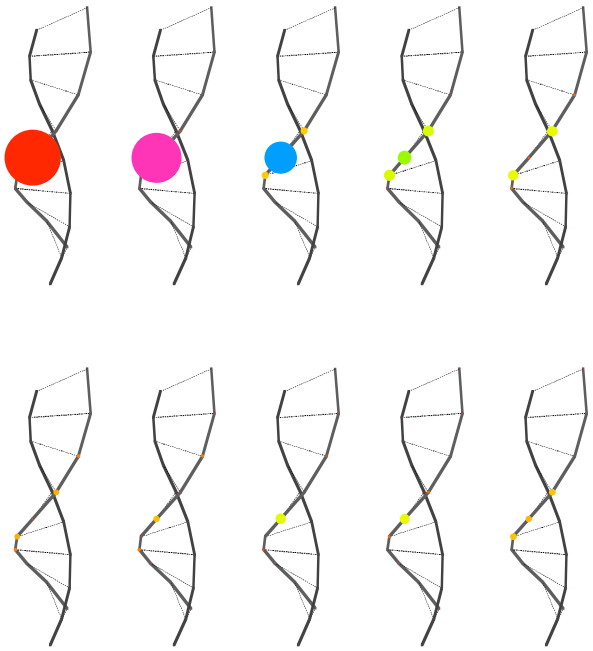

FIG. 10: Exciton probability projected on to DNA sites. The size and hue of the superimposed point is proportional to the probability of finding the exciton on a particular site. Shown are snapshots of the evolution for the first 0 to 90 fs in 10fs steps with the initial state localized on the center most thymidine unit.

50fs, the wavefunction does rebound from the end of the molecule and recurrences are to be expected.

The decay of the initial exciton can be visualized as in Fig. 10 where we project the exciton probability from the numerical calculations onto the three-dimensional coordinates of the sites along the helix. The size and hue of the superimposed dot is indicative of the probability to find the system in a given excitonic configuration along the chain. Each frame following the initial frame in the upper left-hand corner shows the evolution of the exciton wave function in 10fs increments. The reflection of the excitonic wavepacket from the ends of the chain can be clearly seen in the bottom four frames of this figure.

The results in Fig. 11 underscore the importance of the charge-transfer dynamics in these systems. Here, we plot the projection of the time-evolved wavefunction on to all the excitonic configurations and onto only those configurations located on the thymidine chain. Here we see that almost immediately, close to 60% of the initial exciton population has decayed in to non-excitonic configurations with all remaining excitonic population lingering on the original (thymidine) chain. Hence, after the initial excitation, nearly 60% of the original population has dissociated into mobile electron/hole pairs. Moreover, by examining the charge-density as seen in Fig. 12, we find that these electron/hole pairs remain on the original side of the DNA lattice with very little transfer across to the other chain.

In examining Fig. 12 it is interesting to note that once the exciton has broken up in an electron/hole pair, the electron more or less remains pinned to the initial excitation site while the hole moves away more rapidly. This is due to the disparity between the widths of the valence and conduction bands along the thymidine chain. After about 100 fs the electron and hole generated by the excitation have become delocalized across the chain and the net charge density on a given site is close to zero.

Even more detail can be gained by examining the actual time-evolution of the electron/hole wave function. In Fig. 13 we show subsequent snapshots of the electron/hole density starting from the initial exciton placed on the 5th thymidine site and in Fig. 14 we show the electron, hole, net-charge, and exciton density on a given site. What is striking is that within the first 50fs, the exciton has delocalized over the original chain and transfered a small part of its density on to the adenosine immediately adjacent to the originally populated site. In this figure, we plot the logaritm of the density in order to emphasize the more of the features of the evolution. While certainly some interchain transfer is occuring, most of the density remains on the original chain in the form of excitonic (i.e. geminate electron/hole pairs) or charge-separated species. The various curves in Fig. 14 show quantatitively the exciton density on a given site as well as the net charge.

IV. DISCUSSION

In this paper we developed a model for the excited states of DNA based upon the electronic structure of the individual base pairs and their orientation in the DNA polymer strand. This model synthesizes a number of crucial aspects into a common framework that can be used to simulate the ultrafast excited state photophysical dynamics. The model is flexible in that it admits both numerical and analytical solutions for both the conduction and valence bands for the electrons and holes as well as the excited exciton and charge-separated states. The parameters of the model are directly related to specific interactions that can be deduced from either *ab initio* or experimental data. In all, the model is robust and we believe gives a reasonable starting point for describing the short time evolution of photoexcited species.

We emphasize that this model is a starting point for discussion as it is in no means complete nor comprehensive. There are a number of potentially crucial considerations we have neglected at the moment. First and foremost is the neglect of disorder in the model due to the instantaneous fluctuations and gyrations of the DNA chain itself. While DNA is a relatively rigid polymer, especially short segments, torsional and local fluctuations will likely most strongly affect the long-ranged dipole-dipole couplings and the diagonal cross-chain hopping terms present in the conduction and valence band operators as well as in the exciton quasi-particle hamiltonian.

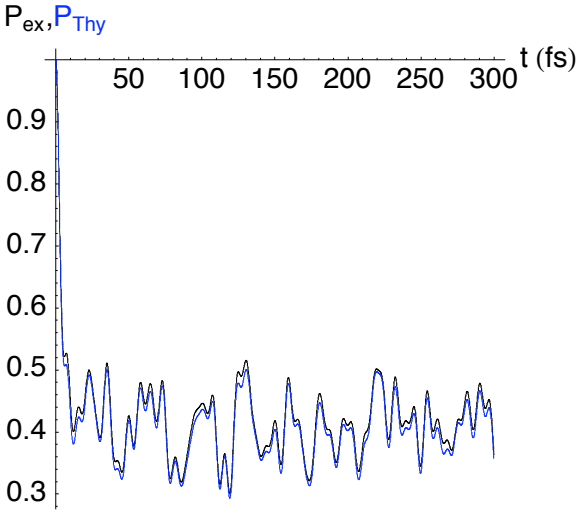

FIG. 11: Probability of finding the system in any excitonic configuration following initial excitation (black) and the probability of finding the system in any excitonic configuration localized only on the thymidine chain (blue). Here we can see that almost immediately 60% the initial population decays into charge-separated (non-excitonic) species while the remaining excitonic density stays on the thymidine chain.

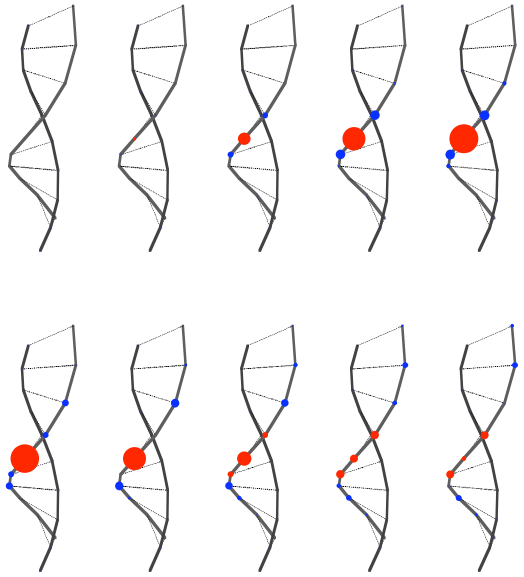

FIG. 12: Net charge on each site following excitation. The size of each superimposed point reflects the magnitude of the charge while color indicates sign (red = negative charge, blue = positive charge). Shown are snapshots of the evolution for the first 0 to 90 fs in 10fs steps with the initial state localized on the center most thymidine unit as in Fig. 10. We see that a significant component of the exciton breaks apart into charge-separated species with the electron remaining localized on the initial site

Such fluctuations will tend to induce localization of the HOMO or LUMO orbitals (as in the case of the valence and conduction bands) and further localize the exciton bands. A second dire approximation is in treating the excitonic coupling within the point-dipole approximation. This approximation is strictly valid when the separation between chromophores is far greater than the relative length scale of the molecules involved. Since the π stacking distance is on the order of 3.4Åin DNA, higer order terms should be included for an accurate assessment of these couplings. Thirdly, we include only a single transition moment for the purines. While there is considerable debate in the literature over these transition moments, the general consensus is that the purines have two transition moments for optical coupling to the ground state both lying in the plane of the molecule pointing in opposite directions. We do not include the effects of dissipation or decoherence within our dynamical model nor do we explicitly include coupling between the electronic and nuclear degrees of freedom. This latter neglect we can justify partially in terms of the Born-Oppenheimer approximation in that the nuclear dynamics corresponding to the large-scale fluctuations of the DNA chain itself occur on a far slower time scale than the the initial electronic dynamics. On the other hand, nuclear coupling

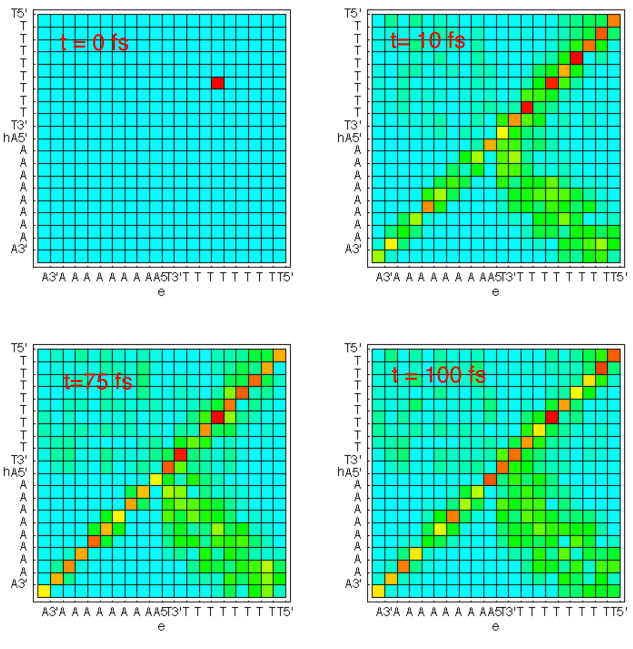

FIG. 13: Evolution of electron/hole wavefunction for first 100 fs given as the natural log of the density.

within the bases themselves play very important roles in dissipating the excitation energy once localization has occurred through conical intersections between the local $\pi\pi^*$ exciton and charge-transfer states. [37, 38, 39] Finally, we have not included the effects of the solvent media nor the dielectric continuum in which the physical DNA molecule resides. This will have the effect of screening any long-range electrostatic interaction and may contribute to the localization or effective mass of mobile charge carriers along the chain itself. For example, Ref. [3] reports that the lifetime of a base-stacked A-T excimer increases by roughly a factor of 2 upon changing the solvent from water to heavy water. On the other hand, no such effect was observed in stacked A-A excimers, so the effect is certainly more pronounced in cases where modulation of the bases generates a modulated redox potential along the chain leading to charge-separated states. [26]

The dynamics implied by our model are quite striking and point towards a crucial interplay between excitonic and charge-transfer dynamics in photoexcited DNA. Because of this, excitonic models alone may not fully account for the initial dynamics and transport of the excited species along the chain. Charge-transfer dynamics arising from the differences between the redox potentials of the different base pairs and the diffences in charge-carrier mobility along a given chain play a role in determining the excitonic vs. charge-separated character of the excited states of the system. Clearly, from the simulations presented in this paper, there is no simple single interaction that one can point to that captures and explains all of the dynamics in these systems. Rather, it is the complex interplay between the various contributions

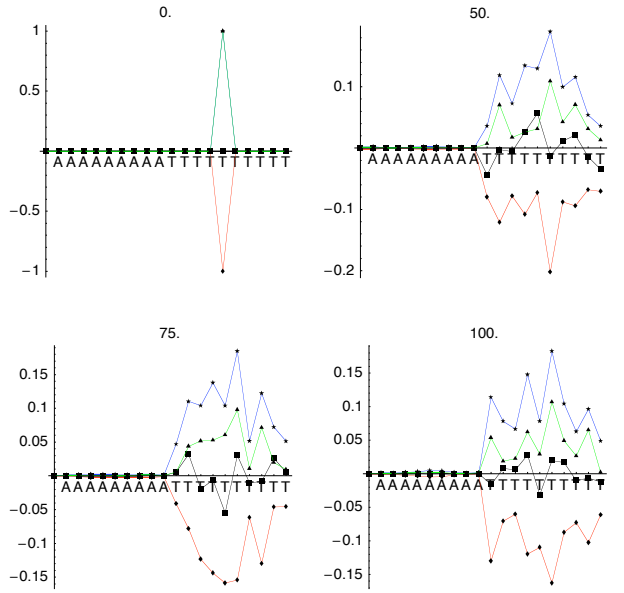

FIG. 14: Evolution of exciton density (green), electron density (red), hole density (blue), and net charge (black) as projected on to each base site. The label on each plot indicates time in fs.

that one needs to assess.

In a broader sense, the localization of the excitation on the initial chain may have played an important role in the evolutionary selection of DNA as the principle genetic courier of all life on Earth. During the early stages of evolution of life on Earth when the primordial atmosphere was considerably less rich in O_2 than today, selection preference would be weighted towards species which could survive in an environment rich in UV light. It is tempting to sepeculate that by localizing *both* excitons and charge-transfer species to the originally photoexcited chain, damage induced by either subsequent photochemical processes, oxydation, or reduction is thereby localized to the original chain leaving the non-excited chain as a "backup copy" of the genetic information.

Acknowledgments

This work was supported in part by grants from the National Science Foundation, the Robert A. Welch Foundation and the Texas Center for Superconductivity (TcSUH). The author also wishes to acknowledge Prof. Stephen Bradforth for conversations and discussions leading to this paper.

[1] J. J. Ladik, Fundamental World of Quantum Chemistry **2**, 271 (2003).

[2] D. Markovitsi, D. Onidas, T. Gustavsson, F. Talbot, and E. Lazzarotto, Journal of the American Chemical Society **127**, 17130 (2005).

[3] C. E. Crespo-Hernandez, B. Cohen, and B. Kohler, Nature **436**, 1141 (2005).

[4] E. Emanuele, D. Markovitsi, P. Millie, and K. Zakrzewska, ChemPhysChem **6**, 1387 (2005).

[5] E. Emanuele, K. Zakrzewska, D. Markovitsi, R. Lavery, and P. Millie, Journal of Physical Chemistry B **109**, 16109 (2005).

[6] F. D. Lewis, Photochemistry and Photobiology **81**, 65 (2005).

[7] F. D. Lewis, X. Liu, Y. Wu, and X. Zuo, Journal of the American Chemical Society **125**, 12729 (2003).

[8] F. D. Lewis, Y. Wu, L. Zhang, X. Zuo, R. T. Hayes, and M. R. Wasielewski, Journal of the American Chemical Society **126**, 8206 (2004).

[9] F. D. Lewis, L. Zhang, X. Liu, X. Zuo, D. M. Tiede, H. Long, and G. C. Schatz, Journal of the American Chemical Society **127**, 14445 (2005).

[10] B. Bouvier, T. Gustavsson, D. Markovitsi, and P. Millie, Chemical Physics **275**, 75 (2002).

[11] E. Conwell, Topics in Current Chemistry **237**, 73 (2004).

[12] D. Dee and M. E. Baur, Journal of Chemical Physics **60**, 541 (1974).

[13] M. Kertesz, Kemiai Kozlemenyek **46**, 393 (1976).

[14] J. Ladik, H. Fruechtl, P. Otto, and J. Jaeger, Journal of Molecular Structure **297**, 215 (1993).

[15] J. Ladik, S. Suhai, P. Otto, and T. C. Collins, International Journal of Quantum Chemistry, Quantum Biology Symposium **4**, 55 (1977).

[16] J. J. Ladik, NATO Advanced Study Institutes Series, Series C: Mathematical and Physical Sciences **C39**, 257 (1978).

[17] Y.-A. Lee, S. Lee, H. M. Lee, C.-S. Lee, and S. K. Kim, Journal of Biochemistry (Tokyo, Japan) **133**, 343 (2003).

[18] T. Miyata and S. Yomosa, Journal of the Physical Society of Japan **27**, 727 (1969).

[19] M. Rist, H.-A. Wagenknecht, and T. Fiebig, ChemPhysChem **3**, 704 (2002).

[20] S. L. Shapiro, A. J. Campillo, V. H. Kollman, and W. B. Goad, Optics Communications **15**, 308 (1975).

[21] M. N. Kobrak and E. R. Bittner, Physical Review B (Condensed Matter and Materials Physics) **62**, 11473 (2000), URL `http://link.aps.org/abstract/PRB/v62/p11473`.

[22] G. C. Claudio and E. R. Bittner, The Journal of Chemical Physics **115**, 9585 (2001), URL `http://link.aip.org/link/?JCP/115/9585/1`.

[23] S. Karabunarliev and E. R. Bittner, Physical Review Letters **90**, 057402 (pages 4) (2003), URL `http://link.aps.org/abstract/PRL/v90/e057402`.

[24] S. Karabunarliev and E. R. Bittner, The Journal of Chemical Physics **118**, 4291 (2003), URL `http://link.aip.org/link/?JCP/118/4291/1`.

[25] S. Karabunarliev and E. R. Bittner, The Journal of Chemical Physics **119**, 3988 (2003), URL `http://link.aip.org/link/?JCP/119/3988/1`.

[26] S. Karabunarliev and E. R. Bittner, J. Phys. Chem. B **108**, 10219 (2004), URL `http://pubs.acs.org/cgi-bin/abstract.cgi/jpcbfk/2004/108/i29/abs/jp036587w.html`.

[27] K. G. Wilson, Phys. Rev. D **10**, 2445 (1974).

[28] J. B. Kogut and L. Susskind, Phys. Rev. D **11**, 395 (1975).

[29] T. Miyata and S. Yomosa, Journal of the Physical Society of Japan **27**, 720 (1969).

[30] H. Mehrez and M. P. Anantram, Phys. Rev. B **71**, 115405 (2005), URL `http://link.aps.org/abstract/PRB/v71/e115405`.

[31] M. W. Schmidt, K. K. Baldridge, J. A. Boatz, S. T. Elbert, M.S.Gordon, J. H. Jensen, S. Koseki, N. Matsunaga, K. A. Nguyen, S. J. Su, et al., J. Comput. Chem **14**, 1347 (1993).

[32] A. Broo and A. Holmen, J. Phys. Chem. A **101**, 3589 (1997).

[33] H. Du, R. A. Fuh, A. Corkan, and J. S. Lindsey, Photochemistry and Photobiology **68**, 141 (1988).

[34] J. W. Longworth, , R. O. Rahn, and R. G. Schulman, J. Chem. Phys. **45** (1966).

[35] A. Pereversev and E. R. Bittner, J. Chem. Phys. **123**, 244903 (2005).

[36] H. Tal-Ezar and R. Kosloff, J. Chem. Phys. **81**, 3967 (1984).

[37] C. Canuel, M. Mons, F. Piuzzi, B. Tardivel, I. Dimicoli, and M. Elhanine, Journal of Chemical Physics **122**, 074316/1 (2005).

[38] A. L. Sobolewski and W. Domcke, European Physical Journal D: Atomic, Molecular and Optical Physics **20**, 369 (2002).

[39] S. Thomas, S. Elena, R. Wolfgang, H. I. V, S. A. L, and D. Wolfgang, Science **306**, 1765 (2004), URL `http://www.sciencemag.org/cgi/content/abstract/306/5702/1765?maxtoshow=&HITS=10&hits=10&RESULTFORMAT=&searchid=1&FIRSTINDEX=0&volume=306&firstpage=1765&resourcetype=HWCIT`.